DOI: 10.1002/ejic.201001101

Further Characterization of the [FeFe]-Hydrogenase Maturase HydG

Cécile Tron,[a,b] Mickaël V. Cherrier,[b,c] Patricia Amara,[b] Lydie Martin,[b] Francois Fauth,[c] Edmundo Fraga,[c] Mélanie Correard,[b] Marc Fontecave,[a,d] Yvain Nicolet,[b] and Juan C. Fontecilla-Camps*[b]

Keywords: Enzymes / [FeFe]-Hydrogenase / Carbon monoxide / Cyanide / Active site maturation

Recent work conducted in several laboratories has shown that the [FeFe]-hydrogenase maturase HydG synthesizes both CO and CN^- from tyrosine. We have very recently found that although CN^- synthesis does not need the [4Fe-4S] cluster found in the HydG C-terminal domain, CO synthesis does require it. We have also proposed that the $^+H_2N^{\cdot}–CH_2–CO_2^-$ radical is a precursor for these two active site ligands. Here, we have extended our characterization of both the wild-type enzyme and a ThiH-like HydG truncated mutant, with small angle X-ray scattering (SAXS) spectroscopy, homology modeling and functional studies.

Introduction

Many microorganisms can catalyze the oxidation of molecular hydrogen or the reduction of protons according to the following reaction: $H_2 = 2H^+ + 2e^-$, thanks to oxygen-sensitive enzymes called hydrogenases.[1] There are two types of enzymes that catalyze this reaction: the [NiFe]-hydrogenases and the [FeFe]-hydrogenases. A third type of enzyme, the [Fe]-hydrogenase, catalyzes only the first step of this reaction, that is, the cleavage of molecular hydrogen into a proton and a hydride.[2] The crystal structures of these proteins have shown that their active sites are complex[1,2] and, not surprisingly, sophisticated maturation machineries involving metal ion transport, the synthesis of organic cofactors, and CN^- and/or CO and the formation and insertion of iron complexes with these triple-bonded ligands, are required for their assembly.[3] The crystal structure of the [FeFe]-hydrogenase from *Desulfovibrio desulfuricans* (*Dd*) showed that in addition to the CN^- and CO ligands, the active site Fe ions are coordinated to a small organic molecule, most likely a bis(thiomethyl)amine (Figure 1).[4,5] Even though the small molecule was not well defined in the first report of the structure of [FeFe]-hydrogenase from *Clostridium pasteurianum* (*Cp*), subsequent work has confirmed its generality.[6] Although the assembly mechanism of the [NiFe]-hydrogenase active site is rather well understood, both functionally and structurally,[3,7] the elucidation of the active site maturation mechanism of its [FeFe] counterpart has been initiated only recently. A major breakthrough in this process occurred in 2004 when Posewitz et al. succeeded in expressing active *Chlamydomonas reinhardtii* (*Cr*) [FeFe]-hydrogenase in *Escherichia coli*.[8]

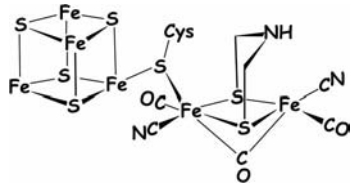

Figure 1. The active site of [FeFe]-hydrogenase. Our initial proposition for the bridgehead atom being N[4] has been subsequently confirmed by spectroscopic studies.[5]

The co-expression of the structural gene *CrHydA* with two additional genes, called *CrHydEF* and *CrHydG*, corresponding to three genes *HydE*, *HydF* and *HydG* in other microorganisms, was found to be both necessary and sufficient to generate active *Cr*HydA hydrogenase. HydE and HydG are radical *S*-adenosyl-L-methionine (SAM or AdoMet) dependent enzymes and HydF displays GTPase activity.[9,10] HydE and HydG are significantly homologous to biotin synthase (BioB) and anaerobic tyrosine lyase (ThiH), respectively.[11] Besides the [4Fe-4S] cluster-containing TIM-barrel domain found, either fully or partially, in all radical SAM enzymes, HydG has additional N- and C-terminal stretches. The latter has three invariant cysteine residues that are coordinated to a second [4Fe-4S] cluster.[10,12]

[a] Laboratoire de Chimie et Biologie des Métaux, Université Joseph Fourier, UMR 5249-CNRS, iRTSV CEA Grenoble, 17, Avenue des Martyrs, 38054 Grenoble Cedex, France
[b] Laboratoire de Cristallographie et de Cristallogenèse des Protéines, Institut de Biologie Structurale J.-P. Ebel. CEA, CNRS, Université Joseph Fourier, 41, Jules Horowitz, 38027 Grenoble Cedex 1, France
Fax: +33-4-38785122
E-mail: juan.fontecilla@ibs.fr
[c] BM16-CRG Consorci Laboratori de Llum de Sincrotró (LLS) c/o ESRF, 38043 Grenoble, France
[d] Collège de France, 11, Place Marcelin-Berthelot, 75005 Paris, France
Supporting information for this article is available on the WWW under http://dx.doi.org/10.1002/ejic.201001101.

Thanks to recent reports from the groups of Swartz, Peters, Broderick, Roach and Happe,[13–19] our understanding of [FeFe]-hydrogenase maturation has significantly improved in recent years; it is now known that the active site H-cluster (Figure 1) is assembled in two steps: the [4Fe-4S] and the dinuclear [FeFe] sub-clusters bind with the apo enzyme in a sequential manner.[16] It has also been reported that in a cell-free synthetic system containing the three essential Hyd maturases, the formation of the [FeFe] sub-cluster is stimulated by tyrosine, cysteine, and SAM.[13]

Our own contribution to this subject has been the determination of the crystal structure of HydE from *Thermotoga maritima* (*Tm*)[20] and the demonstration that, like ThiH,[21] HydG catalyzes the formation of *p*-cresol through the SAM-dependent cleavage of tyrosine (Figure 2).[12] Based on the detection of glyoxylate that is produced from the hydrolysis of dehydroglycine (DHG), and the inhibitory effect of glyoxylate on the tyrosine cleavage by ThiH, Kriek et al. and Challand et al. have postulated that the other product of the reaction is either DHG or the related glycyl radical (Figure 2).[21,22] Soon thereafter, using *Clostridium acetobutylicum* (*Ca*) HydG, Driesener et al.[18] and Shepard et al.[19] showed that tyrosine cleavage by HydG results in the synthesis of both CN^- and CO.

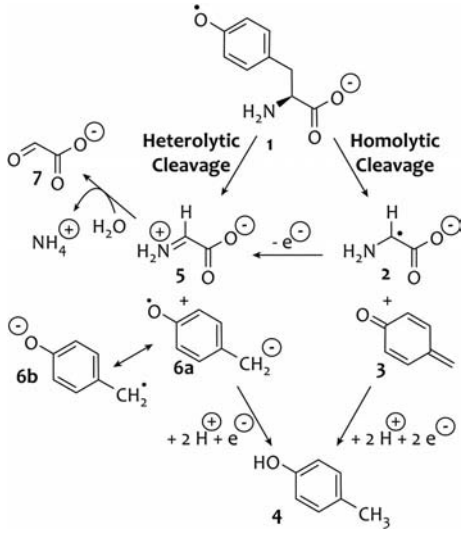

Figure 2. Production of dehydroglycine (**5**) or glycyl radical (**2**) and *p*-cresol (**4**) from tyrosine (**1**) according to Kriek et al.[21] ThiH-derived **5** has been shown to be a precursor for thiazole synthesis.[22] Compound *p*-cresol (**4**) is also made by HydG (see text).[12]

Czech et al.[17] and Shepard et al.[16] have used FTIR spectroscopy to show that after incubation with HydE and HydG, *Ca*HydF carries a binuclear [FeFe] cluster with bound CO and CN^- ligands. The loaded HydF transfers its binuclear cluster to the [4Fe-4S]-containing active site of the hydrogenase HydA generating an active enzyme.[16,17]

Inspired by the finding of King et al., who reported that mutation of any of the three conserved cysteines of the *Ca*HydG C-terminal domain (CTD) resulted in an inactive hydrogenase,[23] we prepared two mutants of *Ca*HydG: one in which two of these cysteines substituted by serine (*Ca*HydG^{SxxS}), and a second in which the 88 residues of the CTD were removed (*Ca*HydG$^{\Delta 88}$).[24] The *Ca*HydG^{SxxS} mutant could still synthesize CN^- but not CO, whereas the *Ca*HydG$^{\Delta 88}$ mutant could not synthesize either ligand. We concluded the following from these results: (1) CN^- synthesis by HydG does not require the C-terminal [4Fe-4S] cluster, but may need some components of the CTD, and (2) CO synthesis requires the CTD [4Fe-4S] cluster. Furthermore, we postulated that the precursor of these two active site ligands is the energetically favored glycyl radical $^+H_2N^{\cdot}–CH_2–CO_2^-$ resulting from tyrosine cleavage.[21,24] Fragmentation of this radical can generate $^{\cdot}CO_2^-$ and $H_2C{=}NH$,[25] which are plausible precursors for CO and CN^-, respectively.[26–28]

Due to some aggregation and the instability of the *Ca*HydG$^{\Delta 88}$ mutant we produced an equivalent truncated *Thermoanaerobacter tengcongensis* (*Tte*) HydG mutant lacking the C-terminal 91-residue domain (*Tte*HydG$^{\Delta 91}$) and modeled it with the known high-resolution three-dimensional structure of HydE.[20] The overall correctness of the partial model, and a possible indication that the N- and C-terminal regions of HydG interact tightly with its TIM-barrel domain, are suggested by the SAXS-generated envelopes for the mutant and wild-type *Tte* proteins. Subsequently, we have used this model to postulate which residues are potentially involved in tyrosine cleavage at the expected substrate-binding site by determining their common conservation in HydG and ThiH.

Finally, we show that the *Ca*HydG$^{\Delta 88}$ and *Tte*HydG$^{\Delta 91}$ truncated mutants produced 1.6% and 1.8% of *p*-cresol relative to their respective wild-type counterparts.

Results and Discussion

Production of *p*-cresol by the *Ca*HydG$^{\Delta 88}$ and *Tte*HydG$^{\Delta 91}$ mutants: In order to determine whether the truncated mutants were able to cleave tyrosine and make *p*-cresol we ran an experiment similar to the one reported by Pilet et al.[12] (see Exp. Section). Although the amount of *p*-cresol produced by the two mutants was small, the HPLC reversed-phase elution profiles of the incubated reaction mixtures showed peaks at 280 nm with both retention times and spectral features that are characteristic of *p*-cresol (Figure 3). The molar response factor determined with commercial *p*-cresol allowed us to establish that the wild-type and truncated *Ca*HydG and *Tte*HydG enzymes produced 2.498 and 0.039 +/– 0.002 mol of *p*-cresol after 2 h, and 2.408 and 0.044 +/– 0.001 mol of *p*-cresol after 1 h per mol of protein, respectively. The reason for the drop in *p*-cresol synthesis is not clear. It could result from either a lower affinity of the truncated *Ca*HydG and *Tte*HydG enzymes for tyrosine binding with respect to the wild type, or a change in the rate of catalysis. However, given the extremely low *p*-cresol production by the *Ca*HydG$^{\Delta 88}$ and *Tte*HydG$^{\Delta 91}$ mutants it is impractical to attempt to measure the K_m and V_{max} values. Consequently, the conclusion from this experiment, the results of which are depicted in Figure 3, is qualitative:

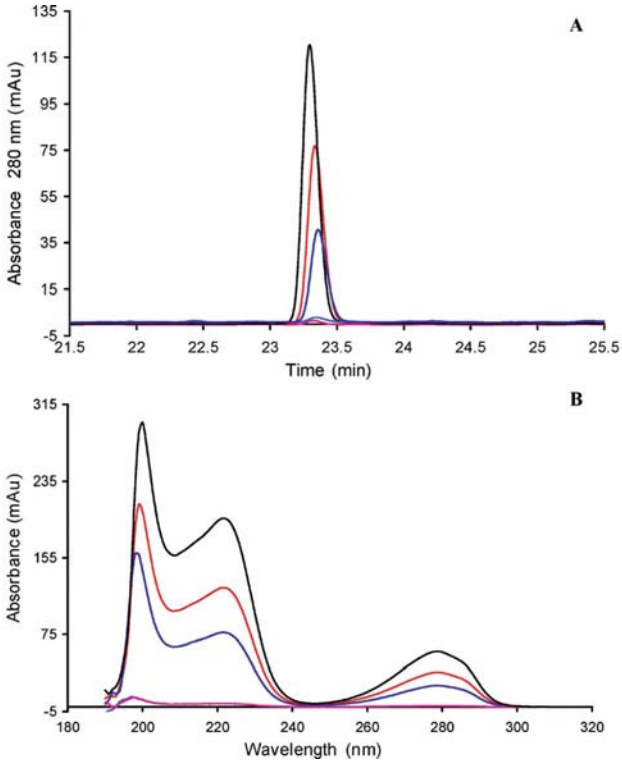

Figure 3. (**A**) HPLC elution profile of *p*-cresol production by wild-type *Ca*HydG (red), its *Ca*HydG$^{\Delta 88}$ mutant (pink), wild-type *Tte*HydG (dark blue), and its *Tte*HydG$^{\Delta 91}$ mutant (light blue). HPLC analysis was carried out with 100 µL and 90 µL reaction volumes for the *C. acetobutylicum* and for the *T. tengcongensis* enzymes, respectively. The elution profile of an injected 10 nmol of *p*-cresol control (black) is also shown. (**B**). The corresponding baseline-corrected UV/Vis spectra depicted as superimposed curves with color codes as in (**A**).

HydG uses its TIM-barrel domain to cleave tyrosine and make *p*-cresol.

What about the nature of the remaining fragment? Using l-U-[^{13}C,^{15}N]tyrosine as a substrate Roach and co-workers[18] have shown that HydG makes CN$^-$ from this amino acid and that *p*-cresol and CN$^-$ were formed in a 1:1 stoichiometry. Additionally, Shepard et al.[19] have used ^{13}C-tyrosine to demonstrate, by FTIR spectroscopy, the production of CO from tyrosine. Quantification of CN$^-$ production by the *Ca*HydG$^{\Delta 88}$ mutant[24] gave the following turnover numbers: 0.03(0) +/– 0.007 for the control without HydG, 1.88 +/– 0.044 for wild-type *Ca*HydG, and 0.04(4) +/– 0.007 for the *Ca*HydG$^{\Delta 88}$ mutant. Given the small amount of *p*-cresol produced by this mutant (Figure 3) it is not surprising to see an insignificant (if any at all) amount of CN$^-$ produced.

Studies of the synthesis of thiazole phosphate have shed considerable light on this problem. Aerobic and anaerobic bacterial thiazole synthetic pathways involve an initial common intermediate obtained from either glycine oxidation (ThiO) or tyrosine cleavage (ThiH), respectively.[22] Park et al. succeeded in replacing aerobic *Bacillus subtilis* ThiO with an excess of glyoxylate and ammonia during in vitro thiazole phosphate synthesis. As glyoxylate and ammonia combine in aqueous solutions to form DHG it can be concluded that this molecule is the first common intermediate in thiazole synthesis by both aerobes and anaerobes.[29] Additional indications that DHG is produced by ThiH were obtained by observing that an excess of glyoxylate prevents tyrosine lyase activity, probably by competitive binding.[22] As the presence of *p*-cresol after the reaction of the truncated HydG with tyrosine implies the production of an ad-

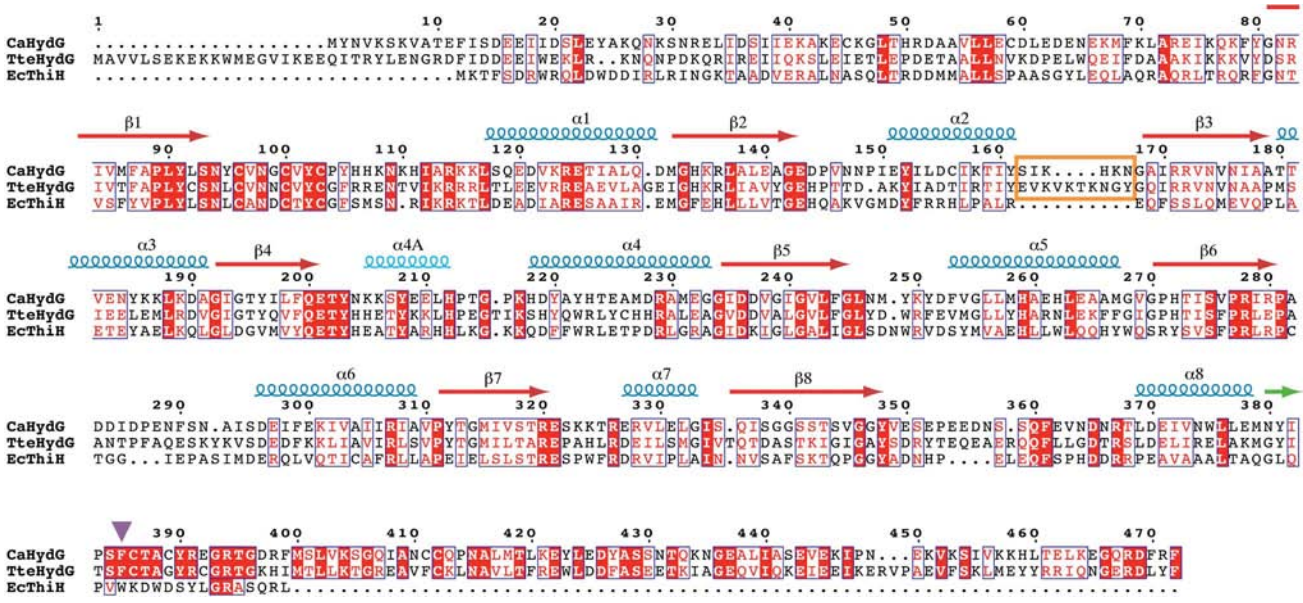

Figure 4. Amino acid sequence comparisons between *Clostridium acetobutylicum* HydG (*Ca*HydG), *Thermoanaerobacter tengcongensis* HydG (*Tte*HydG) and *Escherichia coli* ThiH (*Ec*ThiH). Secondary structure elements corresponding to α-helices (blue loops) and β-strands (red and green arrows) were predicted from the structurally homologous protein HydE from *Thermotoga maritima* according to ref.[10]. The residues inside the brown box correspond to a loop that was difficult to model for *Tte*HydG because it corresponds to a large insertion without an equivalent in the known Radical AdoMet protein structures. In the native HydG structures, this loop may interact with the additional C-terminal domain (see also Figure 5). The purple triangle indicates the position of the stop-codon insertion for the HydG deletion mutants.

ditional fragment [either dehydroglycine or a glycyl radical[21] (Figure 2)], the *Ca*HydG$^{\Delta 88}$ mutant may be considered not only structurally homologous (Figure 4), but also functionally similar to *Ec*ThiH, which lacks the CTD.

Homology modeling of the *Tte*HydG$^{\Delta 91}$ mutant with HydE: A partial three-dimensional model of the truncated *Tte*HydG$^{\Delta 91}$ mutant was built with a combination of structure-based amino acid sequence alignment and loop optimization with the Prime program from the Schrödinger suite.[30] The modeling was restricted to the TIM-barrel domain of HydG, for which the very high-resolution structure of the *Tm*HydE maturase[20] constituted a good starting point. Consequently, both a 50-residue long N-terminal domain and the last 91 C-terminal residues were left out of the model because their structures are not known. As indicated below, the partial theoretical model showed a good fit to a SAXS-generated envelope corresponding to the mutant.

Small-angle X-ray spectroscopic studies with *Tte*HydG$^{\Delta 91}$: The protein from the thermophilic organism was chosen for the SAXS study because it is monodispersed and robust. The radius of gyration (R_g) of *Tte*HydG$^{\Delta 91}$ estimated by the Guinier approximation and the distance distribution function had similar values of 25.4 ± 0.4 and about 24.3 Å, respectively. For *Tte*HydG the estimated Guinier approximation and the distance distribution function also gave similar values of 26.4 ± 0.5 and ca. 24.6 Å, respectively. The SAXS envelope of *Tte*HydG$^{\Delta 91}$ has the general conical shape of its three-dimensional model, confirming that the truncated mutant protein is properly folded in solution (Figure 5, A). The same conclusion can be made in the case of *Tte*HydG (Figure 5, B). The unaccounted for density found in both envelopes near the protein N-terminus corresponds most likely to the 50 residue long N-terminal stretch that is absent from our *Tte*HydG$^{\Delta 91}$ model (Figure 5). An additional electron-dense region is present in the *Tte*HydG envelope below the protein C-terminus (depicted in green in Figure 5, B). According to the peptide property calculator of A. Chazan (www.basic.northwestern.edu/biotools/proteincalc.html), the 91 residues of the C-terminal domain occupy a predicted volume of about 13,000 Å^3 whereas the volume below the C-terminus has an estimated value of about 8,000 Å^3. The difference of 5,000 Å^3 may be explained by the fact that the C-terminal *Tte*HydG [4Fe-4S] cluster is not fully reconstituted in the recombinant enzyme. This, in turn, may introduce excessive flexibility in the C-terminal domain of a significant fraction of protein molecules, reducing the SAXS signal for this region. Experimental scattering curves and the pair distribution function are shown in the Supporting Information.

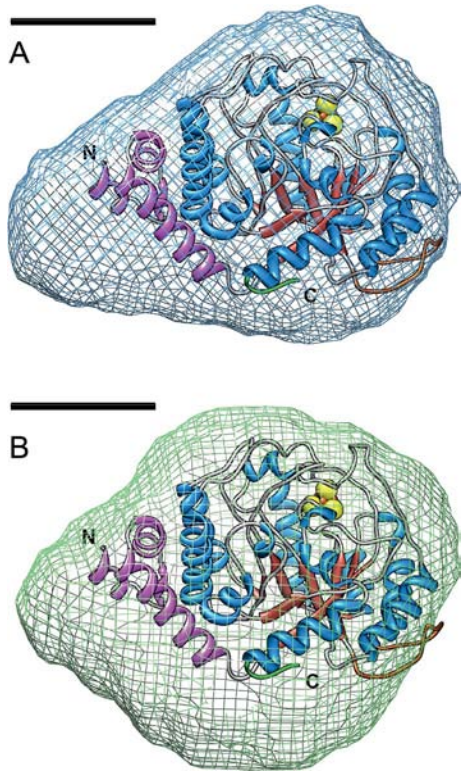

Figure 5. Fit of the *Tte*HydG$^{\Delta 91}$ model into the ab initio determined envelope of *Tte*HydG$^{\Delta 91}$ (blue mesh, A) and *Tte*HydG (green mesh, B) generated with DAMMIF.[31] *Tte*HydG$^{\Delta 91}$ is depicted as a C_α backbone ribbon with helices, sheets and loops colored blue, red and grey, respectively, except for the first three helices, which are colored pink. Residues 180 to 190 and 406 to 410 are colored orange and green, respectively. Yellow and brown spheres represent the [4Fe-4S] cluster. The scale bar represents 25 Å. The N and C labels indicate the N- and C- terminal ends of the partial model, respectively. This graphic was prepared with CHIMERA.[32]

Model-based comparison of *Tte*HydG$^{\Delta 91}$ and *Ec*ThiH: Encouraged by the qualitatively similar catalytic activity of ThiH and the *Tte*HydG$^{\Delta 91}$ mutant,[12] we have examined the conservation of amino acid sequences between these two proteins. This study demonstrates that the comparison between the two enzymes may be divided into three parts: a common "top" region responsible for SAM and the conserved [4Fe-4S] cluster binding, a common "middle" region characteristic of tyrosine binding and cleavage, and a diverging "bottom" region that determines the outcome of its precursors (Figure 6). This comparison confirms the notion that, although both enzymes share a common first step in their respective reactions, the generated precursors follow different paths. During thiazole synthesis, ThiH transfers DHG to ThiG where it becomes a fragment of the 5-(β-hydroxyethyl)-4-methylthiazole phosphate (Thz-P) precursor.[22,29] Conversely, we postulate that HydG uses DHG or the glycyl radical[24] to synthesize CO and CN^-.[18,19]

The distribution of residues in Figure 6 and its comparison with Figure 5 suggest a topological sequence that is relevant to HydG activity. After cleavage of tyrosine by SAM in the region containing potential active site residues (depicted in blue) products are likely to move to the "bottom" of the TIM-barrel domain (residues shown in green). The SAXS envelope for *Tte*HydG (B in Figure 5) suggests that the C-terminal domain binds tightly to that region, and may also interact with the N-terminal domain, placing its [4Fe-4S] cluster close to the cleavage reaction products. The cluster could then further process one of the cleavage products to synthesize CO.[24]

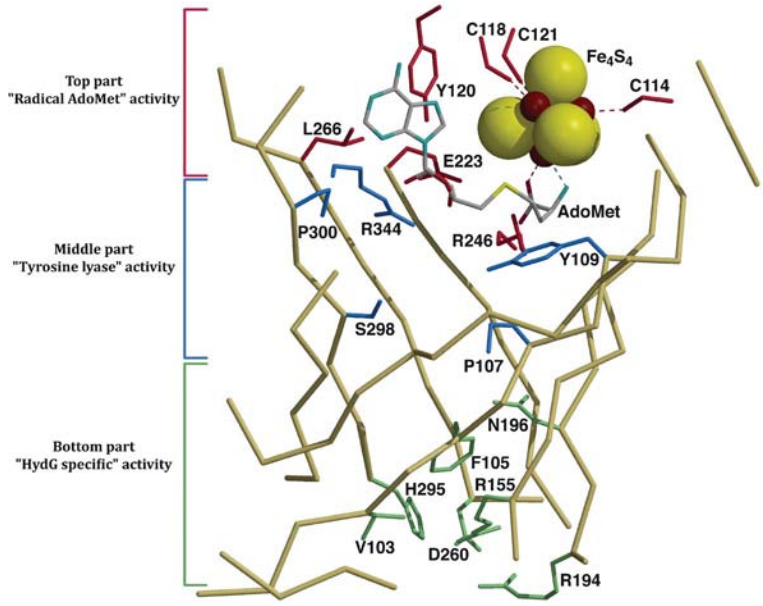

Figure 6. Partial theoretical model of *Tte*HydG$^{\Delta 91}$depicting residues belonging to the "top" region common to SAM radical enzymes (red), the "middle" region with residues common to *Tte*HydG$^{\Delta 91}$and *Ec*ThiH near the active site (blue), and a "bottom" region where the two proteins show no residue conservation (green). Only the β-sheet structure and the residues lining the active site cavity that are strictly conserved are depicted.

Conclusions

Herein we have shown that a truncated version of HydG that lacks the C-terminal domain is still capable of cleaving tyrosine as shown by its *p*-cresol production. However, the removal of this domain significantly reduces the reaction yield when compared to the wild-type enzyme. This may have resulted from exposure to the solvent of some catalytic regions in the TIM-barrel domain. The low *p*-cresol production may also explains the practical absence of CN^- synthesis.[24] We have used the high-resolution crystal structure of HydE to model *Tte*HydG$^{\Delta 91}$ and have verified the overall correctness of the model by fitting it to a SAXS-generated envelope. In addition, in the envelope obtained for the native *Tte*HydG there is excess electron density that, at least partially, may explain the presence of a 50-residue long N-terminal insertion and the contiguous 91-long C-terminal domain, both apparently tightly bound to the TIM-barrel domain. Finally, we have use the model to place (1) those residues likely to be generally involved in [4Fe-4S] cluster and SAM binding, and (2) those that are specific to both HydG and ThiH and are likely to be involved in tyrosine cleavage, and (3) those that may be specific for the next step in the reaction leading towards either CO/CN^-(HydG) or a fragment involved in thiazole synthesis (ThiH). This observation, along with the envelope calculated from a SAXS experiment, suggests a reaction path involving the migration of reaction intermediates from the active site at the middle of the TIM-barrel domain to its bottom and then to the [4Fe-4S] cluster found in the C-terminal domain where CO synthesis is likely to occur.[24]

Experimental Section

Cloning of the HydG gene from *Thermoanaerobacter tengcongensis*: The open reading frame encoding *Tte*HydG (TTE1568) was PCR-amplified with *Caldanaerobacter subterraneus subsp. tengcongensis* DSM 15242 cells (DSMZ), Phusion polymerase (Finnzymes) and the corresponding primers. The N-terminus primer was designed to contain a unique *NdeI* restriction site at the predicted initiation codon (5′- GTAAT***CATATG***GCTGTTGTGCTTAGTGAAAA-3′) and the C-terminus primer to contain a unique *BamHI* site (5′-CATTA***GGATCC***TTAGAAGTAGAGGTCTCTTTCTCCATT-3′). The PCR fragments were purified with the Extract II kit (Macherey–Nagel), digested with *NdeI* and *BamHI* restriction enzymes, and inserted into a pET-15b vector. This construct (pTteHydG) leads to the production of a N-terminal 6His-tagged protein. The *Tte*HydG$^{\Delta 91}$ mutant was obtained following the QuickChange site-directed mutagenesis kit strategy (Stratagene) by introducing a stop codon after position 410 with the pTteHydG construct as a template, Phusion polymerase and the following primers: Forward, 5′-GGGTATATAACAAGTTAGTGCACAGCAGGTTAC-3′; Reverse, 5′-GTAACCTGCTGTGCACTAACTTGTTATATACCC-3′. This process produced the pTteHydG$^{\Delta 91}$ construct. The correctness of the cloned sequences was confirmed by sequencing of the entire genes.

6His-CaHydG, 6His-CaHydG$^{\Delta 88}$, 6His-TteHydG and 6His-TteHydG$^{\Delta 91}$ Protein Expression, Purification and Reconstitution: *Ca*HydG and the truncated *Ca*HydG$^{\Delta 88}$ mutant were expressed and purified as described previously.[24] Plasmids pTteHydG and pTteHydG$^{\Delta 91}$ were used to transform *E. coli* BL21CodonPlus (DE3)-RIL cells (Stratagene) that were grown at 37 °C in TB medium supplemented with 100 mg/L ampicillin and 34 mg/L chloramphenicol. When the OD_{600} reached 0.6, the production of *Tte*HydG and *Tte*HydG$^{\Delta 91}$ was induced by the addition of 1 mM

isopropyl-1-thio-β-D-galactopyranoside to the medium, and the incubation was subsequently carried out at 15 °C overnight in presence of 150 mg/L ferrous ammonium sulfate. Cells were collected by centrifugation at 4000 rpm at 4 °C and stored temporarily at –80 °C. The cell paste was resuspended in buffer A (20 mM Hepes pH 7.5; 500 mM NaCl; 5% glycerol) and disrupted by sonication at 4 °C. Cell debris was removed by centrifugation at 15000 rpm for 45 min. The purification of *Tte*HydG and *Tte*HydG$^{\Delta 91}$ was similar to that of *Ca*HydG and *Ca*HydG$^{\Delta 88}$.[24] The proteins were first purified aerobically by nickel affinity chromatography with a linear gradient of buffer B (20 mM Hepes pH 7.5; 500 mM NaCl; 500 mM imidazole; 5% glycerol). The fractions that were judged to be >90% pure by SDS-PAGE were pooled and dialyzed overnight at 4 °C against buffer C (20 mM Hepes pH 7.5; 500 mM NaCl; 5% glycerol; 5 mM DTT). All subsequent purification steps were similar to those performed for *Ca*HydG and *Ca*HydG$^{\Delta 88}$ and carried out under anaerobic conditions with < 5 ppm O_2. *Ca*HydG, *Ca*HydG$^{\Delta 88}$, *Tte*HydG and *Tte*HydG$^{\Delta 91}$ were reconstituted with Fe^{2+} and S^{2-} in buffer D (20 mM Hepes pH 7.5; 200 mM NaCl; 2 mM DTT) for SAXS experiments or E (20 mM Hepes pH 7.5; 100 mM NaCl) for activity assays, according to Nicolet et al.[24] The reconstituted proteins were stored at –80 °C until use.

HPLC Analysis of SAM- and Tyrosine-Dependent *p*-Cresol Production Activity: Results from this study are depicted in Figure 3. Activity assays were carried out in buffer C in the presence of 20 to 25 μM of enzyme, 2 mM tyrosine, 1 mM *S*-adenosyl-L-methionine. The reaction was initiated with 1 mM sodium dithionite. In the case of *Ca*HydG and *Ca*HydG$^{\Delta 88}$, the samples (final volume 1 mL) were incubated at 30 °C for 2 h, whereas the thermophilic *Tte*HydG and *Tte*HydG$^{\Delta 91}$ samples (final volume 100 μL) were incubated at 55 and 45 °C, respectively, for 1 h.[24] The protein was precipitated with sodium formate at pH 4.3 and 0.35 M final concentration, and *p*-cresol production was analyzed by reverse phase HPLC on a Zorbax 300SB-C18 column (4.6 mm x 250 mm) with a gradient going from 100% of a 0.1% TFA solution to a 50:50 solution of 0.1% TFA and acetonitrile. UV spectra of the peaks corresponding to the retention time of *p*-cresol confirmed the activity of the two wild-type enzymes and the two truncated mutants. The peaks were quantified by converting the area of the HPLC peak with the molar response factor (97.68 +/– 0.09 units of area of *p*-cresol peak detected at 280 nm per mol of *p*-cresol) determined with commercial *p*-cresol (Sigma).

Homology Modeling of the TteHydG$^{\Delta 91}$ Mutant: The mutant model was obtained with the Prime program from the Schrödinger Suite.[30] The sequence of *Tte*HydG was aligned relative to the one of *Tm*HydE. The resulting alignment was modified manually to match secondary structure elements.[11] An initial model for *Tte*HydG$^{\Delta 91}$ was constructed based on the *Tm*HydE crystal structure (3CIW[20]). Loops were refined sequentially and the geometry of the final model was optimized, the cluster and the AdoH in the model retained the conformation that they have in *Tm*HydE.

Note: Loop 180–190 (see Figure 5) could not be optimized further due to the fact that it probably interacts with the missing CTD in the wild-type structure.

SAXS Experiments: These experiments were performed on the BM16-CRG Spanish-operated beam line at the European Synchrotron Radiation Facility (ESRF, Grenoble, France). Data were recorded with a fixed monochromatic X-ray beam (λ = 0.980 Å) and a two-dimensional multi-wire gas detector (90% Xe, 10% CO_2) designed and built at CELLS-ALBA in Barcelona.[33] The sample-detector distance was set to 2,935 mm, covering a 0.024–0.3 $Å^{-1}$ Q-range ($Q = 4\pi sin\theta/\lambda$, with 2θ being the scattering angle) in 0.001 effective steps. The FIT2D software (http://www.esrf.eu/computing/scientific/FIT2D/) was used to process the two-dimensional images to give one-dimensional $I(Q)$ vs. Q patterns.

In order to protect *Tte*HydG from inactivation by air and aggregation, both buffer D (see above) and protein data were collected at 4 °C under anaerobic conditions. A specific cell was designed for this purpose (see Figure S1 in the Supporting Information). It consists of a 3 mm thick polytetrafluoroethylene (PTFE) sheet with a central hole sandwiched between two mica sheets to prevent air contamination. This setup is encased in two 8 mm thick aluminum plates, which are temperature-controlled by a circulating refrigerant fluid. During data collection a continuous nitrogen gas flow was applied on the mica windows in order to prevent water condensation. The sample was introduced in the cell using a syringe, the needle of which was inserted into a vertical hole in the PTFE sheet fitted with an aluminum adaptor connected to a rubber septum (Sigma–Aldrich). *Tte*HydG$^{\Delta 91}$ and *Tte*HydG solutions were concentrated to 2.55 mg/mL and 2.41 mg/mL, respectively.

To monitor any possible aging and/or X-ray induced decay of the samples, 60 exposures of 30 s each were collected from both buffer and protein samples. Possible aggregation was checked for by looking at the Guinier approximation range[34] during data collection. Data were then averaged in order to improve the statistics. The scattering generated by the buffer was subtracted from the protein data. The radius of gyration (R_g) was extracted from the Guinier approximation applied over a Q range of 0.024–0.0475 $Å^{-1}$ (23 points) for both *Tte*HydG and *Tte*HydG$^{\Delta 91}$. The R_g value was also extracted from the pair distance function $P(r)$ calculated by the program GNOM,[35] with a D_{max} of 70 Å for both *Tte*HydG and *Tte*HydG$^{\Delta 91}$.

To calculate a low-resolution model of the protein we used DAMMIF,[31] an improved version of the ab initio bead-modeling program DAMMIN.[36] Fifteen models were generated with DAMMIF and subsequently averaged with DAMAVER.[37] The *Tte*HydG$^{\Delta 91}$ model was fitted to the SAXS-generated envelope excluding the 180–190 loop because it was too long to be properly modeled (see Figures 5 and 6). Using the program COLORES from the SITUS package[38] we obtained six plausible fits for the modeled truncated HydG to the SAXS envelope. The first four solutions were equivalent (normalized cc = 0.99 relative to the first solution); the first model is depicted in Figure 5 (A). In the fifth solution the model was rotated 180° along an approximately horizontal axis, as shown in the Figure, and the normalized cc = 0.98. The sixth solution was clearly erroneous (normalized cc = 0.95). In the first four solutions there is room for the N-terminal 50-residue long domain missing from the model (see Figure 5, A). In the case of the wild-type HydG, the truncated model could not be used for the fitting procedure because it is too incomplete (besides the N-terminal domain and the C-terminal domains are also missing). Consequently, the envelope corresponding to the wild-type enzyme was fitted to the one obtained for the truncated mutant using the program CHIMERA[32] and the model was oriented accordingly (Figure 5, B). In both cases there is room for the N-terminal fragment and, at least partially, for the C-terminal domain. The scattering curves and pair distance function for *Tte*HydG and *Tte*HydG$^{\Delta 91}$ are shown in the Supporting Information.

Supporting Information (see footnote on the first page of this article): Supporting Information is provided for the SAXS experiments.

Acknowledgments

We thank Dr. E. Mulliez for his generous gift of SAM and S. Arragain for advice with *p*-cresol detection. This work was financed by the French Agence Nationale pour la Recherche (contract ANR-08-BLAN-0224-01).

[1] J. C. Fontecilla-Camps, A. Volbeda, C. Cavazza, Y. Nicolet, *Chem. Rev.* **2007**, *107*, 4273–4303.
[2] T. Hiromoto, K. Ataka, O. Pilak, S. Vogt, M. S. Stagni, W. Meyer-Klaucke, E. Warkentin, R. K. Thauer, S. Shima, U. Ermler, *FEBS Lett.* **2009**, *583*, 585–590.
[3] A. Bock, P. W. King, M. Blokesch, M. C. Posewitz, *Adv. Microb. Physiol.* **2006**, *51*, 1–71.
[4] Y. Nicolet, A. L. de Lacey, X. Vernede, V. M. Fernandez, E. C. Hatchikian, J. C. Fontecilla-Camps, *J. Am. Chem. Soc.* **2001**, *123*, 1596–1601.
[5] A. Silakov, B. Wenk, E. Reijerse, W. Lubitz, *Comments Mod. Phys. Comments Mod. Phys. Phys. Chem. Chem. Phys.* **2009**, *11*, 6592–6599.
[6] Y. Nicolet, B. J. Lemon, J. C. Fontecilla-Camps, J. W. Peters, *Trends Biochem. Sci.* **2000**, *25*, 138–143.
[7] A. K. Jones, O. Lenz, A. Strack, T. Buhrke, B. Friedrich, *Biochemistry* **2004**, *43*, 13467–13477.
[8] M. C. Posewitz, P. W. King, S. L. Smolinski, L. P. Zhang, M. Seibert, M. L. Ghirardi, *J. Biol. Chem.* **2004**, *279*, 25711–25720.
[9] J. K. Rubach, X. Brazzolotto, J. Gaillard, M. Fontecave, *FEBS Lett.* **2005**, *579*, 5055–5060.
[10] X. Brazzolotto, J. K. Rubach, J. Gaillard, S. Gambarelli, M. Atta, M. Fontecave, *J. Biol. Chem.* **2006**, *281*, 769–774.
[11] Y. Nicolet, C. L. Drennan, *Recent Dev. Nucleic Acids Res.* **2004**, *32*, 4015–4025.
[12] E. Pilet, Y. Nicolet, C. Mathevon, T. Douki, J. C. Fontecilla-Camps, M. Fontecave, *FEBS Lett.* **2009**, *583*, 506–511.
[13] J. M. Kuchenreuther, J. A. Stapleton, J. R. Swartz, *Plos One* **2009**, 4.
[14] S. E. McGlynn, S. S. Ruebush, A. Naumov, L. E. Nagy, A. Dubini, P. W. King, J. B. Broderick, M. C. Posewitz, J. W. Peters, *J. Biol. Inorg. Chem.* **2007**, *12*, 443–447.
[15] S. E. McGlynn, E. M. Shepard, M. A. Winslow, A. V. Naumov, K. S. Duschene, M. C. Posewitz, W. E. Broderick, J. B. Broderick, J. W. Peters, *FEBS Lett.* **2008**, *582*, 2183–2187.
[16] E. M. Shepard, S. E. McGlynn, A. L. Bueling, C. S. Grady-Smith, S. J. George, M. A. Winslow, S. P. Cramer, J. W. Peters, J. B. Broderick, *Proc. Natl. Acad. Sci. USA* **2010**, *107*, 10448–10453.
[17] I. Czech, A. Silakov, W. Lubitz, T. Happe, *Proc. FEBS Meet. FEBS Lett.* **2010**, *584*, 638–642.
[18] R. C. Driesener, M. R. Challand, S. E. McGlynn, E. M. Shepard, E. S. Boyd, J. B. Broderick, J. W. Peters, P. L. Roach, *Angew. Chem. Int. Ed.* **2010**, *49*, 1687–1690.
[19] E. M. Shepard, B. R. Duffus, S. J. George, S. E. McGlynn, M. R. Challand, K. D. Swanson, P. L. Roach, S. P. Cramer, J. W. Peters, J. B. Broderick, *J. Am. Chem. Soc.* **2010**, *132*, 9247–9249.
[20] Y. Nicolet, J. K. Rubach, M. C. Posewitz, P. Amara, C. Mathevon, M. Atta, M. Fontecave, J. C. Fontecilla-Camps, *J. Biol. Chem.* **2008**, *283*, 18861–18872.
[21] M. Kriek, F. Martins, M. R. Challand, A. Croft, P. L. Roach, *Angew. Chem. Int. Ed.* **2007**, *46*, 9223–9226.
[22] M. R. Challand, F. T. Martins, P. L. Roach, *J. Biol. Chem.* **2010**, *285*, 5240–5248.
[23] P. W. King, M. C. Posewitz, M. L. Ghirardi, M. Seibert, *J. Bacteriol.* **2006**, *188*, 2163–2172.
[24] Y. Nicolet, L. Martin, C. Tron, J. C. Fontecilla-Camps, *FEBS Lett.* **2010**, *584*, 4197–4202.
[25] M. Bonifacic, I. Stefanic, G. L. Hug, D. A. Armstrong, A. Klaus-Dieter, *J. Am. Chem. Soc.* **1998**, *120*, 9930–9940.
[26] J. Grodkowski, P. Neta, *J. Phys. Chem. B* **2001**, *105*, 4967–4972.
[27] M. Diefenbach, M. Bronstrup, M. Aschi, D. Schroder, H. Schwarz, *J. Am. Chem. Soc.* **1999**, *121*, 10614–10625.
[28] W. R. Johnson, J. C. Kang, *J. Org. Chem.* **1971**, *36*, 189–192.
[29] J. H. Park, P. C. Dorrestein, H. Zhai, C. Kinsland, F. W. McLafferty, T. P. Begley, *Biochemistry* **2003**, *42*, 12430–12438.
[30] *Prime version 2.2*, Schrödinger, LLC, New York, NY **2010**.
[31] D. Franke, D. I. Svergun, *J. Appl. Crystallogr.* **2009**, *42*, 342–346.
[32] E. F. Pettersen, T. D. Goddard, C. C. Huang, G. S. Couch, D. M. Greenblatt, E. C. Meng, T. E. Ferrin, *J. Comput. Chem.* **2004**, *25*, 1605–1612.
[33] I. Ramos-Lerate, D. Beltran, I. Magrans, J. C. Martinez, J. A. Perlas, J. Bordas, *Nucl. Instrum. Methods Phys. Res. Sect. A* **2003**, *513*, 197–200.
[34] A. Guinier, *Small-angle scattering of X-rays*, John Wiley & Sons, New York **1955**.
[35] D. I. Svergun, *J. Appl. Crystallogr.* **1992**, *25*, 495–503.
[36] D. I. Svergun, *Biophys. J.* **1999**, *76*, 2879–2886.
[37] V. V. Volkov, D. Svergun, *J. Appl. Crystallogr.* **2003**, *36*, 860–864.
[38] W. Wriggers, *Biophys. Rev. Lett.* **2010**, *2*, 21–27.

Received: October 15, 2010
Published Online: February 2, 2011

